MDPI

Article

Unveiling the Influence of Activation Protocols on Cobalt Catalysts for Sustainable Fuel Synthesis

M. Amine Lwazzani [1], Andrés A. García Blanco [1], Martí Biset-Peiró [1], Elena Martín Morales [1] and Jordi Guilera [1,2,*]

[1] Catalonia Institute for Energy Research (IREC), Jardins de Les Dones de Negre 1, 08930 Sant Adrià de Besòs, Spain
[2] Facultat de Química, Universitat de Barcelona, Martí i Franquès, 1, 08028 Barcelona, Spain
* Correspondence: jguilera@irec.cat

Abstract: The Fischer–Tropsch Synthesis process is projected to have a significant impact in the near future due to its potential for synthesizing sustainable fuels from biomass, carbon dioxide and organic wastes. In this catalytic process, catalyst activation plays a major role in the overall performance of Fischer–Tropsch Synthesis. Catalyst activation temperatures are considerably higher than the typical operating conditions of industrial reactors. Consequently, ex situ activation is often required for industrial Fischer–Tropsch Synthesis processes. This study evaluated the influence of different activation approaches (in situ, ex situ, passivation and low-temperature activation). Catalytic experiments were conducted in a fixed-bed reactor at 230 °C and 20 bar·g using a reference supported Co/γ-Al_2O_3 catalyst. Experimental results demonstrate that catalysts can be effectively reduced ex situ. This work reveals that re-activation of the catalyst after ex situ reduction is unnecessary, as the reaction conditions themselves re-reduce any superficial oxides formed, owing to the reducing nature of the reactant mixture. This approach could simplify reactor design by enabling temperature requirements to match operating conditions (e.g., 230 °C), thereby reducing both investment and operational costs and eliminating additional catalyst preparation steps.

Keywords: Fischer–Tropsch Synthesis; cobalt catalyst; reduction; catalyst activation; reactor design

1. Introduction

The Fischer–Tropsch Synthesis (FTS) process plays a pivotal role in gas-to-liquid (GtL) technology, transforming synthesis gas derived from natural gas [1–4]; coal gasification [1–4]; CO_2 co-electrolysis [5,6]; or reverse water–gas shift (r-WGSR) [1,3,5,6] into long-chain hydrocarbons applicable as fuels and lubricants [7–11]. Nowadays, the need for the electrification of industrial processes has increased the interest in the production of sustainable fuels obtained from renewable energy sources, water and CO_2 (e-fuels). These fuels have gathered increasing interest as they can supply a sustainable, climate-neutral alternative in hard-to-abate sectors such as maritime and aviation transportation. As the global demand for cleaner energy sources increases, FTS derived from biogenic synthesis gas has garnered substantial interest due to its potential for producing environmentally friendly fuels with reduced sulfur content [5,12,13]. The use of cobalt-based catalysts in FTS has become especially prominent, given cobalt's ability to selectively produce long-chain hydrocarbons with high activity and stability under synthesis conditions. These characteristics are crucial for industrial applications where maximizing yield and catalyst lifetime are key economic drivers.

Traditionally, the industrial-scale application of Fischer–Tropsch Synthesis faces challenges due to reactor operation [1,5,14–16], where the temperature and flow gradients are minimized by the design of optimized setups such as the slurry bubble and multitubular reactors [14–17]. However, new emerging reactor technologies such as the honeycomb

configurations [17–19], micro-structured reactors [18,19] and CANs® technology [20–25] have focused on optimizing these operating variables by intensifying the cooling and heat transfer of these devices [1,5,14–19,26]. A successful FTS performance requires an effective activation of the catalyst. The activation process involves reducing metal oxides (e.g., CoO, Co_3O_4 or Fe_2O_3) to their metallic forms (Co or Fe), which is achieved at higher temperatures than the operating FTS temperature for which the reactors are designed. To solve this setback, ex situ reduction—pre-activating the catalyst outside the reactor before introducing it into the system—emerges as an accepted industrial solution, as seen in the patent literature [27–29].

Industrially, the catalyst is fully reduced ex situ at temperatures between 350–450 °C [4, 30–35] with specialized equipment and then passivated, at low temperatures, to create a protective oxide layer that is reversed by a lower-temperature reduction [4]. The application of this method minimizes reactor temperature requirements and can potentially reduce investment costs, energy consumption and overall catalyst degradation, ultimately enhancing the economic viability of FTS plants [36]. By improving the cost-efficiency and operational performance, ex situ reduction could serve as a valuable strategy in advancing the economic feasibility of Fischer–Tropsch-based GtL processes [4].

The effects of the sintering and degradation of catalysts are generally debated, apart from reduction treatments [37,38], while the performance of passivated catalysts is rarely discussed [4]. Fratalocchi et al. [4] demonstrated that passivated catalysts exhibit a limited shelf life; although their catalysts could resist air oxidation well up to one week, they started to show degradation symptoms after one month of air exposure and, furthermore, after six months they showed complex reduction behaviors.

Notably, one of the limitations found in the literature is the lack of comparisons in catalytic behavior between standard in situ treatments and ex situ treatments. In this paper, we activated a reference cobalt catalyst through different approaches and characterized their active surface by DRIFTS altogether with evaluating their catalytical performance in the FTS synthesis. Ex situ reduction, passivation and low-temperature activation approaches were evaluated and contrasted to in situ reduction in order to unveil the influence of the activation protocols on sustainable fuel synthesis.

2. Results

2.1. Catalyst Properties

Table 1 shows the composition, skeletal density, surface area, pore volume and average pore diameter of the unreduced catalyst. The metallic content of the catalyst was determined in 14.5 wt.% for cobalt by ICP. The surface area, pore volume and diameter were measured at 141 m^2/g, 0.35 cm^3/g and 10 nm, respectively. FESEM and EDX images of cross-sectioned catalyst pellets were taken to analyze the location of Co inside the pellets. Figure 1 shows that Co was homogeneously distributed along the catalyst pellet.

Table 1. Physical characterization of the unreduced catalyst.

Co	Skeletal Density	Surface Area	Pore Volume	Pore Diameter	Co_3O_4 Particle Size
[wt%]	[g/cm^3]	[m^2/g]	[cm^3/g]	[nm]	[nm]
14.5	3.49	141	0.35	10.0	27

The XRD diffraction patterns of the unreduced and reduced catalysts, ExP, In and Ex, are depicted in Figure 2. The unreduced catalyst showed a main narrow diffraction peak at 36.84° identified as the crystallite phase Co_3O_4 (ICDD Card No. 00-043-1003). Small peaks of this crystallite phase, at ca. 19.00°, 31.27°, 44.81°, 59.35° and 65.23°, were also detected. The unreduced catalyst only showed the presence of the Co_3O_4 oxide form, implying a totally oxidized state. Diffractograms of the ExP, In and Ex catalysts revealed that Co_3O_4 was not present in their crystalline phases, as the Co_3O_4 was fully transformed into metallic Co and CoO (ICDD cards No. 00-015-0806 and No. 01-070-2857, respectively).

The different reduction procedures led to the same result, as Co_3O_4 was fully reduced into Co and CoO. The metallic Co mainly exhibited one main peak at 44.40°, while the CoO oxide exhibited three strong peaks at 36.62°, 42.76° and 61.92°. The Ex sample was exposed to atmospheric oxygen at ambient conditions after XRD measurement to assess the effect of air oxidation (Figure 3). The results revealed that metallic cobalt remained present in the sample even after 48 h of air exposure and the Co_3O_4 phase was still undetected after 48 h. Detailed information relative to the crystalline particle sizes and post-reaction diffractograms can be found in the Supplementary Materials. The crystalline particle sizes of the catalysts revealed that particle sizes remained consistent for most samples after reaction, except for the In sample, which showed a significant increase. Additionally, post-reaction diffractograms indicated the presence of new peaks in the 20–30° range, attributed to carbonaceous species, with no evidence of the Co_3O_4 phase observed.
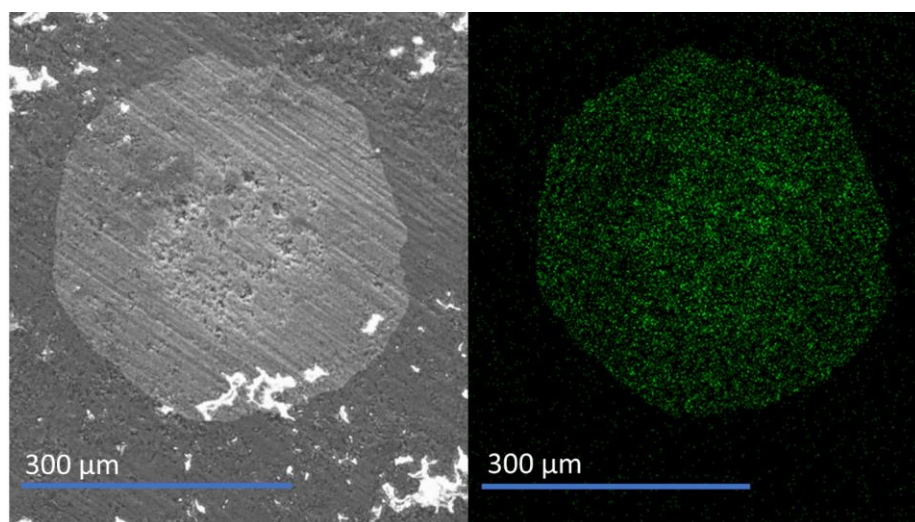

Figure 1. (**Left**) Cross-section of the reference Co catalyst under electron microscopy. (**Right**) Mapping of the Co presence, in yellow spots, in the same catalyst particle.
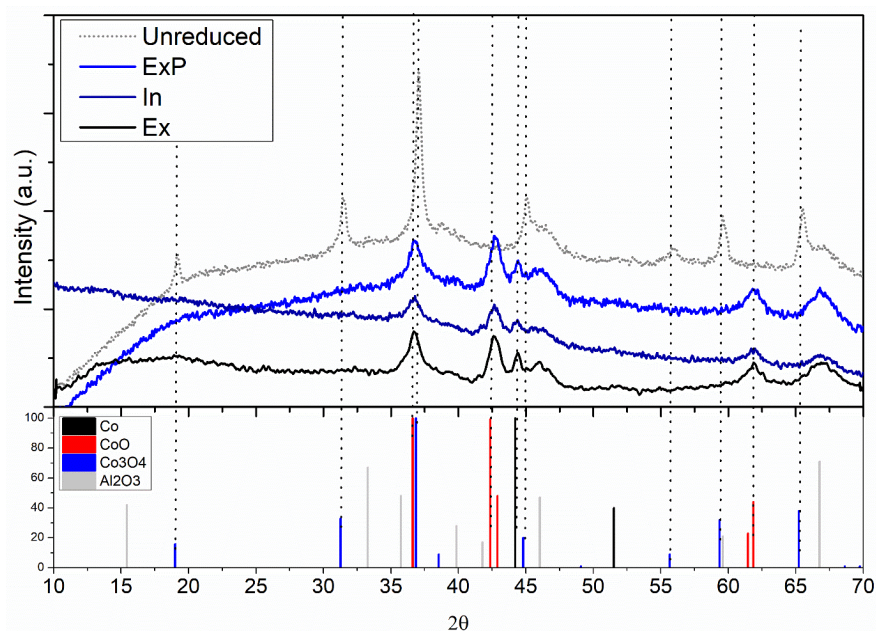

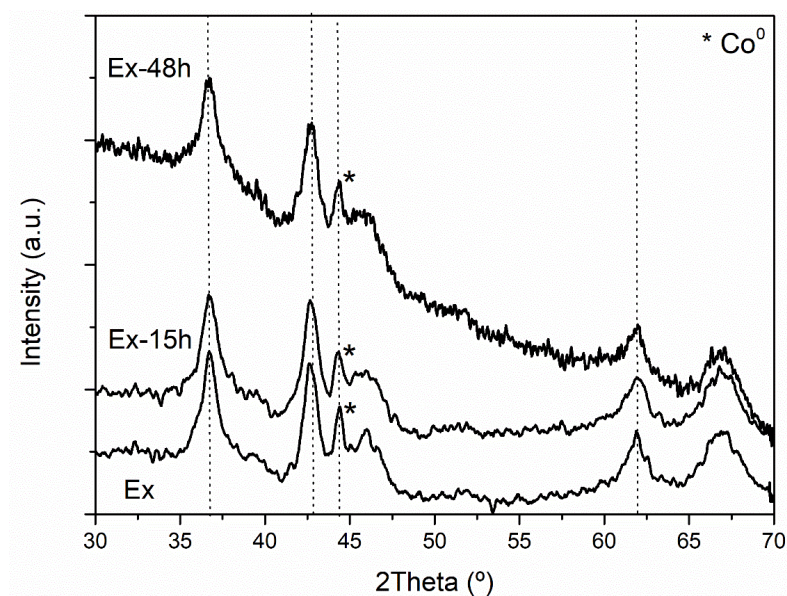**Figure 2.** XRD diffraction patterns of the catalyst samples.

Figure 3. XRD of the ex situ reduced sample after 15 and 48 h air exposition. * represents the metallic Co peak.

Figure 4 shows the H_2-TPR results of the unreduced catalyst and the ex situ reduced (Ex) catalysts with different pre-treatments (ExP and ExPA). The Ex sample shows two main H_2 consumption peaks, with a first peak in the range 230–280 °C associated with the low-temperature reduction of cobalt oxides [2,39,40] and a second one, in the range 450–550 °C, which is assigned to the formation of hard-to-reduce Co species (cobalt aluminates) [4,41]. The cobalt oxide reduction occurs in two stages, in which the first reduction of Co_3O_4 to CoO takes place at 230–260 °C [33], followed by the reduction of the CoO to metallic cobalt (260–350 °C) [39,40]. The presence of the low-temperature peak suggests that mainly CoO species are formed during air exposure of the sample [4].

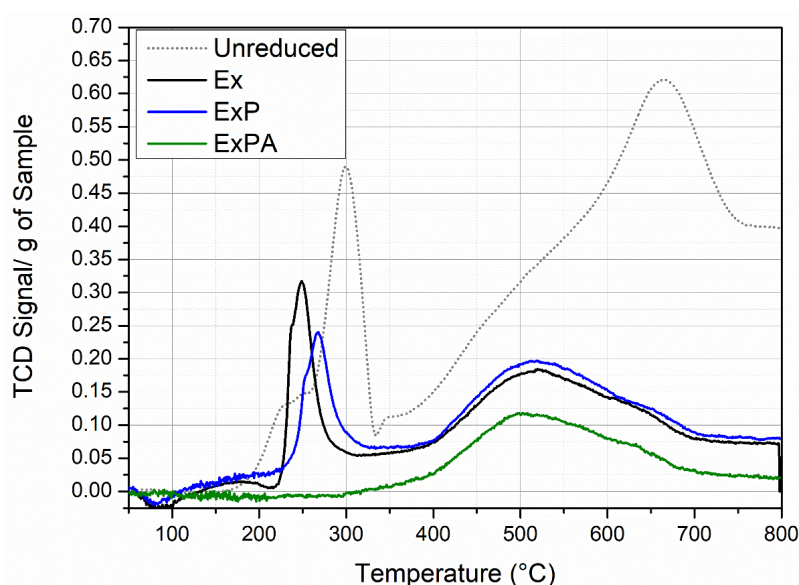**Figure 4.** TPR profiles of the reduced catalysts.

It is also observed that both the Ex and ExP exhibit reduction peaks, including a low-temperature reduction peak at ~240–280 °C, which indicates partial re-oxidation of both materials after exposure to air, be it while material manipulation (i.e., discharging and reactor loading) (Ex) or by the passivation mixture, with later contact with oxygen

(ExP). The differences in the area below the curves in comparison with the Ex sample suggest a partial oxidation, as was also observed in the XRD results. After performing the in situ low-temperature activation at 250 °C (ExPA sample) the low-temperature peak disappears, confirming the effectiveness of this treatment for the reduction (and activation) of the catalyst.

In addition, several changes are observed in the low-temperature reduction region after the ex situ reduction treatment. The most relevant is that the maximum of the peak is shifted towards low temperatures (~240–260 °C) after the ex situ reduction, allowing activation at lower temperatures than the initial unreduced sample (380 °C). Additionally, changes in the characteristics of the low-temperature peak for the ExPA and ExA samples suggest different characteristics of the oxides formed with or without passivation.

The materials were further characterized using CO chemisorption, which revealed notable differences in active metallic surface areas among the catalysts (Table 2). The In catalyst, reduced directly in the TPR equipment, exhibited the highest metallic area (5.65 m^2/g_{sample}). In contrast, the ExA and ExPA catalysts, reduced ex situ and subsequently activated in the equipment before the chemisorption experiments, exhibited significantly lower metallic areas. The metallic area of the ExA sample (2.57 m^2/g_{sample}) was less than half that of the In sample, while the ExPA sample displayed even smaller values. From CO chemisorption data, the activation protocols for the ExA and ExPA catalysts appear insufficient to restore the active metallic surface area achieved through in situ reduction.

Table 2. CO Chemisorption measurements of the catalytic samples.

ID	Active Metallic Surface Area
	$[m^2/g_{sample}]$
In	5.65
ExA	2.57
ExPA	0.70

DRIFTS was used as a tool for characterizing the active surface sites after the different activation treatments performed to the samples. The bands in the 2250–1700 cm^{-1} range correspond to CO adsorbed on a distribution of heterogeneous sites [42–45]. Chemisorbed CO (linear at 2050–2020 cm^{-1}, bridged CO at 1930 cm^{-1} and polycarbonyl at 1868 cm^{-1}) species are direct evidence of the potential activity of the catalysts, since CO dissociation on the surface of metallic Co is the rate-determining step of CO hydrogenation [42,44]. Figure 5 shows that the Ex and ExP samples, without previous activation, do not show peaks of chemisorbed CO. This fact indicates surface oxidation of the samples despite the observed reduced species detected in the bulk by XRD. After applying low-temperature treatment under H_2 atmosphere at 250 °C, peaks assigned to chemisorbed CO (linear, bridged and polycarbonyl) appeared, indicating that this treatment is effective in removing (partially) the oxide layer that is passivating the surface of the catalysts. Hence, these results demonstrate that activating the ex situ reduced samples (ExA and ExPA) at lower temperatures (250 °C) than the required for the first reduction (380 °C) is possible for obtaining an active surface for CO chemisorption. As a reference, a sample (In) was reduced in situ in the DRIFT cell at 380 °C and the corresponding DRIFT spectra show an intense peak of chemisorbed CO species.
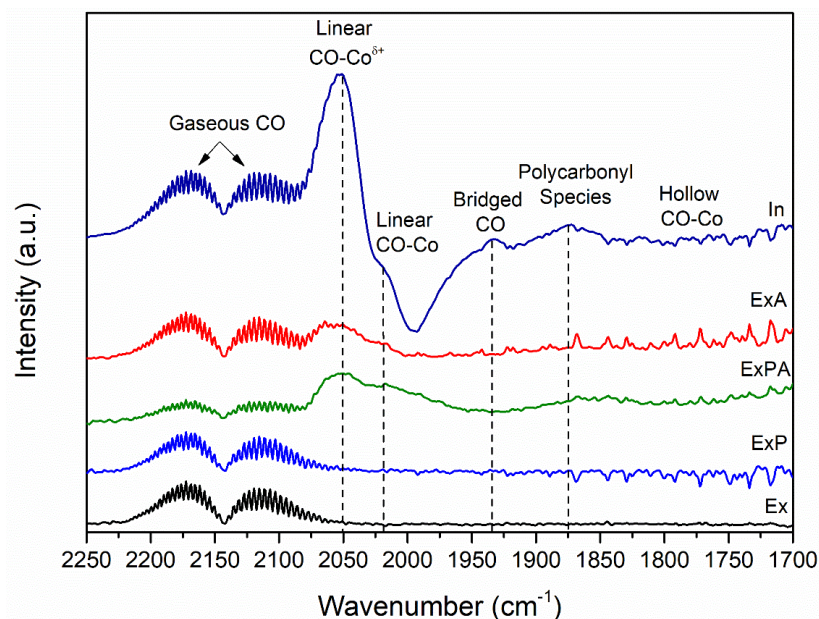
Figure 5. DRIFT spectra of the different reduction procedure samples.

2.2. Catalytic Tests

The characterization results confirm the feasibility of reducing the catalysts ex situ by transforming the Co_3O_4 into CoO and Co, as seen by the XRD results. Moreover, after activation at a low temperature (250 °C), a flattening of the cobalt oxide peak was measured by TPR. The catalysts were loaded in the reactor and and subjected to different spatial velocities to assess their conversions. The obtained catalytic results are shown in Figure 6.
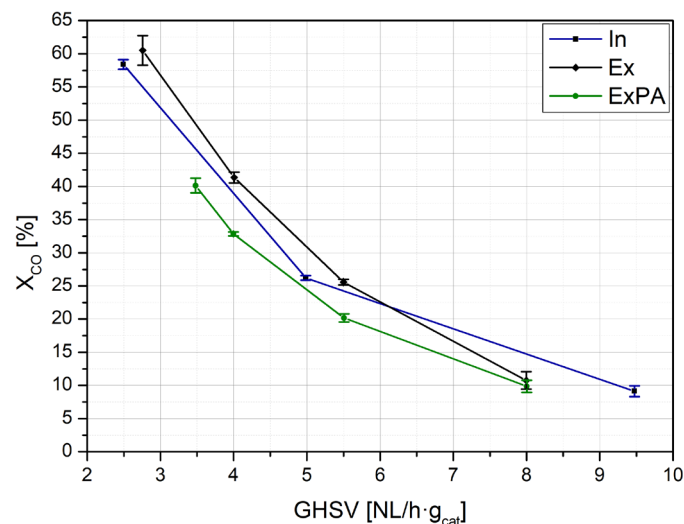

Figure 6. Conversion results of the reduced catalysts under FTS conditions, 20 bar·g and 230 °C.

It is observed that the catalys samples show similar performance in the FTS, validating the effectiveness of the different ex situ procedures performed. The passivation and its later low-temperature activation (ExPA) did not show enhancements compared to the non-passivated sample (Ex), as both showed similar performance under the FTS conditions ($X_{CO} \pm 10\%$). Another relevant observation is that the ex situ reduced catalyst that was exposed to air without prior passivation treatment (Ex) was active under the FTS conditions without previous activation at 250 °C. The CO chemisorption results revealed significant differences in the active metallic surface area of the In, ExA and ExPA catalysts, whilst the catalytic results showed comparable behavior at similar conditions. These results suggest

that the activation procedure is insufficient to fully reduce the catalysts, while the reaction conditions could correctly activate the catalysts. The activation of the Ex sample under synthesis conditions offers great potential for process optimization and time management by reducing the need for successive catalyst conditioning steps.

When the Ex catalyst was characterized by different techniques, it showed the presence of CoO and no CO chemisorption capacity before activation. Therefore, in situ DRIFTS under reaction conditions (H_2/CO feed, 230 °C) was performed for this sample to assess the evolution of its surface upon catalytic conditions. The DRIFTS recorded after 0.5 and 5 h of reaction (Figure 7) confirm that the Ex catalyst is correctly re-reduced and activated under reaction conditions, as seen by the multiple carbonyl species adsorbed on the cobalt species. Therefore, from both catalytic activity and CO chemisorption behaviors, the activation of samples under synthesis conditions seems a promising approach.
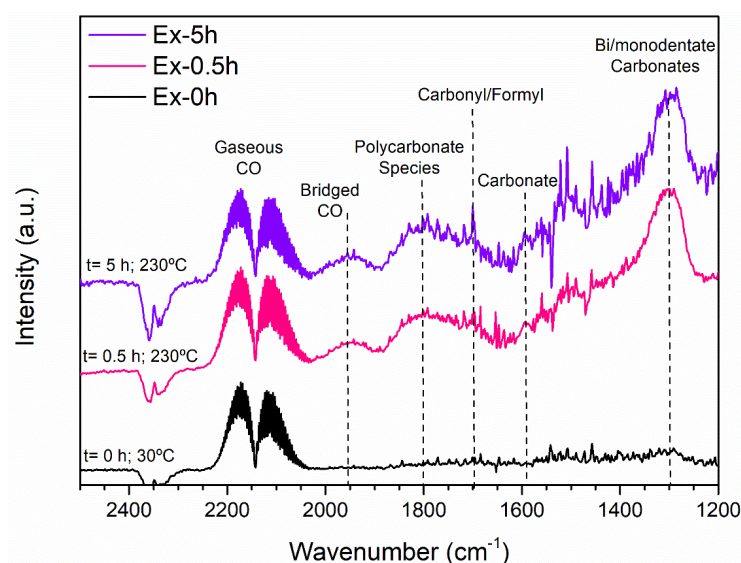

Figure 7. DRIFT of the ex situ catalyst under reaction conditions showing active CO chemisorption sites.

One of the main threats of reducing the FTS catalysts under syngas conditions is the production of carbon deposits that lower the catalytic activity [4,38] of the materials and favor methane production [38]. However, the superficial oxidation and re-reduction of the active surface was effectively undergone under syngas (2:1 ratio H_2/CO *v/v*), showing equivalent activity compared to the in situ reduction under pure hydrogen when comparing the CO conversions without compromising the catalyst stability (detailed information is given at the Supplementary Materials). In addition, the syngas activation effect on methane selectivity was contrasted by comparing the results for the In, Ex and ExPA catalysts (Figure 8). Notably, the methane selectivity of the ex situ samples was slightly lower than the reference in situ sample, where the ExPA catalyst showed the lowest methane selectivity, especially at low spatial velocities.

Previous studies [37,38] highlighted the effect of the reduction–oxidation–reduction processes on cobalt particle size; they reported that more stable catalysts are obtained due to the rearrangement of the cobalt particles into uniformly distributed particle sizes, contrasting the heterogeneous distributions attained by the direct reduction of the catalysts. Regarding the effect of the cobalt particle size on the FTS performance, Bezemer [46] reported that small cobalt particles, below 6 nm, show higher activity and higher methane selectivity than the larger ones. Therefore, the slightly lower activity and lower methane selectivity can plausibly be attributed to the more uniform particle size resulting from the reduction–oxidation–reduction process, simulated by the passivation and subsequent activation of the ExPA catalyst.
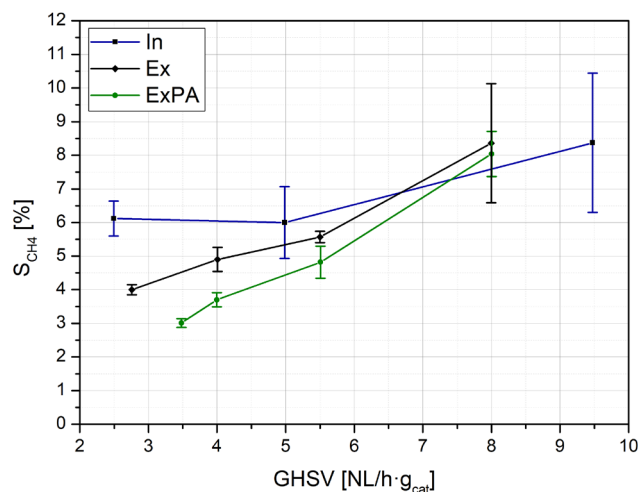
Figure 8. Methane Selectivity of the catalysts.

The main advantages of the ex situ compared to in situ reduction lies in the possibility to optimally produce reduced catalyst batches in optimized furnaces configurations, eliminating the need to over-engineer FTS reactors to withstand high temperatures (>350 °C). FTS reactors are designed primarily to dissipate the substantial heat generated by the highly exothermic reactions, rather than to provide additional heating. Additionally, conducting the reduction ex situ streamlines logistics and facilitates process optimization by utilizing dedicated, smaller-scale equipment designed specifically for this purpose. Although the reduction temperature remains the same, the difference in volumes, process times, total energy consumption and operational costs of the operation are significant. Thus, this approach not only minimizes energy consumption but also improves the overall process flow and operational efficiency of the plant.

3. Experimental

3.1. Catalyst Synthesis

A cobalt catalyst ($Co/\gamma\text{-}Al_2O_3$) was synthesized by a conventional wet impregnation method. Cobalt nominal composition was fixed at 15 wt.%. Cobalt(II) nitrate hexahydrate [$Co(NO_3)_2 \cdot 6\,H_2O$, $\geq 98\%$, Merck Life Science S.L.U., Madrid, Spain] was used as cobalt precursor. A commercial alumina support ($\gamma\text{-}Al_2O_3$, 500 μm spheres, Norpro Saint-Gobain, Stow, OH, USA) was used and dried overnight at 105 °C. The precursor solution was added onto the pre-dried support, the remaining wet sample was dried in a rotary evaporator under vacuum at 80 °C and soft rotation. Afterward, the impregnated material was dehydrated overnight at 105 °C and calcined at 275 °C (heating rate: 2 °C·min^{-1}) for 5 h under static air conditions.

3.2. Reduction, Passivation and Activation Procedures

In situ and ex situ activation procedures were implemented with the aim of reducing cobalt metal oxides (CoO and Co_3O_4) into the metallic form (Co). The first approach consisted of the in situ reduction of the catalyst in a microactivity fixed-bed reactor (Stainless steel AISI 316, Microactivity Reference, PID Eng&Tech, Alcobendas, Spain), 30 cm total reactor length; 17.5 cm usable length; and 0.8 cm internal diameter (Microactivity Reference, PID Eng&Tech, Alcobendas, Spain), considered as the reference.

In the ex situ approach, the reduction was conducted in a tube furnace equipped with a quartz reactor (40 mm external diameter and 65 cm tube length, Carbolite, Hope, Derbyshire, UK) placed into a tubular electric furnace (Carbolite, Hope, Derbyshire, UK). Mass flow controllers were used to regulate the flow rates of the reactants and reduction temperature inside the quartz reactor was fixed at 380 °C. Catalysts were cooled down after ex situ reduction to room temperature under the H_2/Ar reduction gas mixture.

After cooling, catalysts were either passivated or directly discharged in a hexane-filled flask for oxygen-exposure minimization. Passivated catalysts were thereafter activated at 250 °C in the microactivity reactor. After catalyst activation, the system was cooled to 160 °C under hydrogen flow. When attained, the system was purged with the reactive mixture (2:1 H_2/CO syngas and 5% *v/v* N_2) for 20 min before pressurizing the reactor to 20 bar·g. Chromatograms were taken at these conditions (160 °C and 20 bar·g) until stable measurement. Posteriorly, the reactor was led to reaction conditions (230 °C and 20 bar·g). Samples and reduction procedure conditions are detailed in Table 3.

Table 3. Detailed procedure description of the reduction, passivation and activation procedures.

Sample	Procedure	Gas Mixture	Flow	Heating Rate	Final Temperature	Dwell
		[*v/v*]	[NmL/min]	[°C/min]	[°C]	[h]
Unreduced	-	Air	-	-	Room	-
(In)	In situ	H_2	48	1	380	3 h
(Ex)	Ex situ	H_2/Ar 5%	400	1	380	3 h
(ExA)	Ex situ	H_2/Ar 5%	400	1	380	3 h
	Activation	H_2	48	1	250	16 h
(ExP)	Ex situ	H_2/Ar 5%	400	1	380	3 h
	Passivation	O_2/N_2 1%	200	-	Room	8 h
(ExPA)	Ex situ	H_2/Ar 5%	400	1	380	3 h
	Passivation	O_2/N_2 1%	200	-	Room	8 h
	Activation	H_2	48	1	250	16 h

Consequently, the names of the samples indicate the different procedure abbreviations applied. For instance, ExPA means an ex situ reduced sample, passivated and activated, while the unreduced sample implies a non-treated sample.

3.3. Characterization Techniques

Scanning electron microscopy (SEM) micrographs and elemental composition of the samples were obtained using a field emission scanning electron microscope (FESEM, (Zeiss, Oberkochen, Germany) equipped with an energy-dispersive X-ray spectrometer (EDX, Oxford x-Max, Oxford Instruments, Abingdon, UK). For EDX mapping, the particles of the catalyst were cold-drawn in epoxy resin and left to cure for 24 h. The specimens were then polished to obtain the cross-section of the sphere sand coated by gold sputtering.

The chemical composition of the catalyst (Al and Co) was determined by inductively coupled plasma with atomic emission spectroscopy (ICP-AES) in an Optima Perkin Elmer 3200 RL apparatus (Perkin Elmer, Shelton, CT, USA). The skeletal density of the catalyst was measured in a Quantachrome Micro Ultrapyc 1200e Automatic Gas Pycnometer (Boynton Beach, FL, USA). Skeletal density was measured by passing helium at 20 psig pressure to the unreduced sample. Textural properties were determined from N_2-physisorption (adsorption/desorption) isotherms measured in a TriStar II 3020-Micromeritics sorption analyzer (Micromeritics, Norcross, GA, USA). The surface area was calculated from N_2 adsorption data using the BET theory. The crystallite phases in the materials were studied by powder X-ray Diffraction (XRD), measured in a XRD D8 Advance A25 diffractometer (Bruker, Preston, Australia). The average crystallite size was calculated using Scherrer's equation: $dCo_3O_4 = (K\lambda/\beta Cos\theta)$, where λ is the X-ray wavelength, β is the full width of the diffraction line at half maximum (FWHM) and θ is the Bragg angle.

The reducibility of the catalysts was analyzed by temperature-programmed reduction (H_2-TPR) on an Autochem 2890 (Micromeritics, Norcross, GA, USA); conditions were 50 NmL·min^{-1} of H_2 flow (12 vol% H_2/Ar) at 10 °C·min^{-1} rate. While measuring the

reducibility of the samples by the TPR, the samples were subjected to the same reduction procedures described before, nonetheless, activation of the ExA sample was performed in the TPR at 250 °C under H_2 flow. The metal surface area was determined by pulsed CO chemisorption in the same equipment used for the TPR experiments. Prior to a chemisorption measurement, each sample was reduced according its procedure. CO uptake was measured by injecting CO pulses through a calibrated on-line sampling valve (0.5215 cm^3 10%CO/He) until saturation was attained.

In situ Diffuse Reflectance Infrared Fourier Transform Spectroscopy (DRIFTS) was used in order to obtain information about the surface-active sites for CO chemisorption. DRIFTS experiments were performed at ambient pressure with a high-temperature DRIFTS cell (Harrick Scientific Corporation, Pleasantville, NY, USA) fitted with ZnSe windows, using a collector assembly (Praying MantisTM, Bruker, Preston, Australia). The spectrophotometer used was a Vertex 70 (Bruker, Preston, Australia) fitted with a liquid N_2-cooled DigiTect MCT-detector (Bruker, Preston, Australia). DRIFT spectra were recorded with 2 cm^{-1} of spectral resolution and an average of 200 scans per spectrum. Mass flow controllers were used to ensure the composition of the gaseous stream mixtures. After loading the catalyst in the IR cell, Ar and H_2 were flushed at 30 °C under the flow of 20 and 18 NmL·min^{-1} respectively, while a reference spectrum was collected at 400 scans (2 cm^{-1} spectral resolution). Afterwards, a pulse composed of 2 NmL·min^{-1} of CO was flushed for 5 min. The evolution of surface species under the H_2/Ar mixture (20 NmL·min^{-1} of Ar and of 18 NmL·min^{-1} of H_2) was measured just after the CO pulse. The conditions of in situ reduction (In sample) and activation (-A samples) were reproduced inside the DRIFT chamber, while the ex situ reduction and passivation were carried out as indicated before (see Table 1).

Once the samples were characterized by the CO pulse, a fresh sample of the ex situ catalyst (Ex) was loaded on the device to evaluate its performance under FTS gas mixture conditions. (20 NmL/min H_2 and 20 NmL/min 10% *v*/*v* CO/He). A reference spectrum was collected at a 2 cm^{-1} resolution with 200 scans at room temperature. Afterward, the sample was heated to 230 °C at a 10 °C/min rate, while recording spectra every 30 min for 5 h.

3.4. Catalytic Test Procedure

Fischer–Tropsch catalytic studies were carried out at 230 °C and 20 bar·g in a fixed-bed reactor (Microactivity Reference, PID Eng&Tech, Alcobendas, Spain). Syngas (33.13% CO; 66.7% H_2, Linde) and N_2 (99.999%, Linde) were used in each catalytic run. Effluent gases were analyzed online with an online gas micro-chromatograph (μGC) equipped with a TCD (490 microGC, Agilent Technologies, Santa Clara, CA, USA). Experiments were conducted using 0.5 g of catalyst particles. The reaction for each spatial velocity was maintained for at least 4 h while the total duration of the experiment was carried out for at least 20 h (more detailed information is found in the Supplementary Materials). N_2 was used as an internal standard within the reactant mixture that was introduced in the reactor while the pressure was raised up to 20 bar·g. After pressure was reached, multiple injections were made to obtain the blank values for conversion calculation [Equation (1)]. The standard deviations for the conversion and selectivity were below 2.5%; further information about the reaction behavior can be found in the SI.

CO and H_2 conversion (X_i) were calculated according to Equation (1):

$$X_i(\%) = \frac{F_{i,o} - F_i}{F_{i,o}} \times 100 \tag{1}$$

where $F_{i,o}$ is the molar flow rate of species *i* before reaction and F_i is the molar flow at the outlet, considering the internal standard in the effluent stream. Selectivity to methane (S_{CH4}) was calculated according to Equation (2):

$$S_{CH4} = \frac{F_{CH4}}{F_{CO,0} - F_{CO}} \times 100 \tag{2}$$

The *GHSV* was altered to obtain different CO conversions after internal standard. Normalized flow was measured as gas-hourly spatial velocity (*GHSV*), calculated as shown in Equation (3):

$$GHSV = \frac{F_{syn}}{m_{cat}} \tag{3}$$

where the *GHSV* is defined in terms of $NL \cdot h^{-1} \cdot g_{cat}^{-1}$. F_{syn} is the total syngas flow in $NL \cdot min^{-1}$ and m_{cat} is the catalyst mass in g.

4. Conclusions

The activation of cobalt-based catalysts is crucial for optimal FTS performance. Experimental results demonstrate that catalysts can be effectively reduced ex situ and then used in the FTS reaction. Notably, this work reveals that re-activation of the catalyst after ex situ reduction is unnecessary, as the reaction conditions themselves re-reduce any superficial oxides formed, thanks to the reactant mixture. The ex situ reduced samples showed activity comparable to the reference in situ catalyst, with the added benefit of slightly lower methane selectivity compared to the in situ procedure. However, the suitability of passivation and subsequent activation is limited, resulting in only slightly lower methane selectivity. These conclusions may have significant implications for industrial FTS, as the catalyst can be prepared ex situ and directly used in the reactor without further treatment. This approach could simplify FTS reactor design by enabling temperature requirements to match operating conditions (e.g., 230 °C), thereby lowering both investment and operational costs and eliminating additional catalyst preparation steps.

Supplementary Materials: The following supporting information can be downloaded at: https://www.mdpi.com/article/10.3390/catal14120920/s1, Table S1–S3: Crystalline Particle Size (nm) of the prepared samples. Crystalline Particle Size after 15 h and 48 h air exposure. Mean and standard deviation (%) of the Conversion and methane selectivity. Figures S1–S7: XRD of the samples before and after reaction. TOS of the In sample. TOS of the Ex sample. TOS of the ExPA sample. TOS of the methane selectivity for the In sample. TOS of the methane selectivity for the Ex sample. TOS of the methane selectivity for the ExPA sample.

Author Contributions: M.A.L.: Writing—original draft, Methodology, Investigation, Formal analysis, Conceptualization. A.A.G.B.: Writing—original draft, Validation, Formal analysis, Conceptualization. M.B.-P.: Writing—review and editing, Validation, Methodology. E.M.M.: Writing—review and editing, Validation, Methodology. J.G.: Writing—original draft, Validation, Funding acquisition, Formal analysis, Conceptualization. All authors have read and agreed to the published version of the manuscript.

Data Availability Statement: The data supporting the findings of this study, including characterization and detailed catalytic results, are available in the article's Supplementary Information or available under request.

Conflicts of Interest: The authors declare no conflicts of interest.

References

1. Apolinar-Hernández, J.E.; Bertoli, S.L.; Riella, H.G.; Soares, C.; Padoin, N. An Overview of Low-Temperature Fischer–Tropsch Synthesis: Market Conditions, Raw Materials, Reactors, Scale-Up, Process Intensification, Mechanisms, and Outlook. *Energy Fuels* **2024**, *38*, 1–28. [CrossRef]
2. Clarkson, J.; Ellis, P.R.; Humble, R.; Kelly, G.J.; McKenna, M.; West, J. Deactivation of Alumina Supported Cobalt FT Catalysts during Testing in a Continuous-Stirred Tank Reactor (CSTR). *Appl. Catal. A Gen.* **2018**, *550*, 28–37. [CrossRef]

3.   Díaz-López, J.A.; Guilera, J.; Biset-Peiró, M.; Enache, D.; Kelly, G.; Andreu, T. Passivation of Co/Al2O3 Catalyst by Atomic Layer Deposition to Reduce Deactivation in the Fischer–Tropsch Synthesis. *Catalysts* **2021**, *11*, 732. [CrossRef]

4.   Fratalocchi, L.; Groppi, G.; Visconti, C.G.; Lietti, L.; Tronconi, E. On the Passivation of Platinum Promoted Cobalt-Based Fischer-Tropsch Catalyst. *Catal. Today* **2020**, *342*, 79–87. [CrossRef]

5.   Sun, C.; Pfeifer, P.; Dittmeyer, R. One-Stage Syngas-to-Fuel in a Micro-Structured Reactor: Investigation of Integration Pattern and Operating Conditions on the Selectivity and Productivity of Liquid Fuels. *Chem. Eng. J.* **2017**, *326*, 37–46. [CrossRef]

6.   Panzone, C.; Philippe, R.; Chappaz, A.; Fongarland, P.; Bengaouer, A. Power-to-Liquid Catalytic CO_2 Valorization into Fuels and Chemicals: Focus on the Fischer-Tropsch Route. *J. CO_2 Util.* **2020**, *38*, 314–347. [CrossRef]

7.   Metzger, D.F.; Klahn, C.; Dittmeyer, R. Downsizing Sustainable Aviation Fuel Production with Additive Manufacturing—An Experimental Study on a 3D Printed Reactor for Fischer-Tropsch Synthesis. *Energies* **2023**, *16*, 6798. [CrossRef]

8.   Brynolf, S.; Hansson, J.; Anderson, J.E.; Skov, I.R.; Wallington, T.J.; Grahn, M.; Korberg, A.D.; Malmgren, E.; Taljegård, M. Review of Electrofuel Feasibility—Prospects for Road, Ocean, and Air Transport. *Prog. Energy* **2022**, *4*, 042007. [CrossRef]

9.   Su-ungkavatin, P.; Tiruta-Barna, L.; Hamelin, L. Biofuels, Electrofuels, Electric or Hydrogen?: A Review of Current and Emerging Sustainable Aviation Systems. *Prog. Energy Combust. Sci.* **2023**, *96*, 101073. [CrossRef]

10. Meurer, A.; Kern, J. Fischer–Tropsch Synthesis as the Key for Decentralized Sustainable Kerosene Production. *Energies* **2021**, *14*, 1836. [CrossRef]

11. Balli, O.; Caliskan, N.; Caliskan, H. Aviation, Energy, Exergy, Sustainability, Exergoenvironmental and Thermoeconomic Analyses of a Turbojet Engine Fueled with Jet Fuel and Biofuel Used on a Pilot Trainer Aircraft. *Energy* **2023**, *263*, 126022. [CrossRef]

12. Sandford, C.; Malins, C. *Vertical Take-Off? Cost Implications and Industrial Development Scenarios for the UK SAF Mandate*; ICCT The Internation Council on Clean Transportation: Washington, DC, USA, 2024. Available online: https://theicct.org/wp-content/uploads/2024/08/ID-155-%E2%80%93-UK-SAF_final.pdf (accessed on 15 October 2024).

13. Dry, M.E. The Fischer–Tropsch Process: 1950–2000. *Catal. Today* **2002**, *71*, 227–241. [CrossRef]

14. Sie, S.T.; Krishna, R. Fundamentals and Selection of Advanced Fischer–Tropsch Reactors. *Appl. Catal. A Gen.* **1999**, *186*, 55–70. [CrossRef]

15. Avci, A.K.; Önsan, Z.I. (Eds.) *Multiphase Catalytic Reactors: Theory, Design, Manufacturing, and Applications*; John Wiley & Sons Inc.: Hoboken, NJ, USA, 2016; ISBN 978-1-118-11576-3.

16. Méndez, C.I.; Ancheyta, J.; Trejo, F. Modeling of Catalytic Fixed-Bed Reactors for Fuels Production by Fischer–Tropsch Synthesis. *Energy Fuels* **2017**, *31*, 13011–13042. [CrossRef]

17. Xue, Y.; Duan, S.; Chao, K.; Zhang, M.; Li, K.; Ding, Y.; Cheng, K.; Liu, Z.; Chen, J. Construction of Honeycomb-like Hematite Superstructure on Fe Foam and Their Application in Fischer–Tropsch Synthesis. *J. Mater. Sci.* **2024**, *59*, 2841–2851. [CrossRef]

18. Almeida, L.C.; Echave, F.J.; Sanz, O.; Centeno, M.A.; Arzamendi, G.; Gandía, L.M.; Sousa-Aguiar, E.F.; Odriozola, J.A.; Montes, M. Fischer–Tropsch Synthesis in Microchannels. *Chem. Eng. J.* **2011**, *167*, 536–544. [CrossRef]

19. Guettel, R.; Kunz, U.; Turek, T. Reactors for Fischer-Tropsch Synthesis. *Chem. Eng. Technol.* **2008**, *31*, 746–754. [CrossRef]

20. Peacock, M.; Paterson, J.; Reed, L.; Davies, S.; Carter, S.; Coe, A.; Clarkson, J. Innovation in Fischer–Tropsch: Developing Fundamental Understanding to Support Commercial Opportunities. *Top. Catal.* **2020**, *63*, 328–339. [CrossRef]

21. Collins, J.P.; Font Freide, J.J.H.M.; Nay, B. A History of Fischer-Tropsch Wax Upgrading at BP—From Catalyst Screening Studies to Full Scale Demonstration in Alaska. *J. Nat. Gas Chem.* **2006**, *15*, 1–10. [CrossRef]

22. Scaling up SAF Production with Fischer Tropsch Technology. Available online: https://www.hydrocarbonprocessing.com/news/2024/04/scaling-up-saf-production-with-fischer-tropsch-technology/ (accessed on 12 November 2024).

23. Johnson Matthey and Bp Technology Chosen for the World's Largest Fischer Tropsch SAF Production Plant. Available online: https://matthey.com/media/2024/dg-fuels (accessed on 12 November 2024).

24. CANS-Novel-Reactors. Available online: https://matthey.com/products-and-markets/chemicals/cans-novel-reactors (accessed on 12 November 2024).

25. Font Freide, J.J.H.M.; Collins, J.P.; Nay, B.; Sharp, C. A History of the BP Fischer-Tropsch Catalyst from Laboratory to Full Scale Demonstration in Alaska and Beyond. In *Studies in Surface Science and Catalysis*; Davis, B.H., Occelli, M.L., Eds.; Fischer-Tropsch Synthesis, Catalyst and Catalysis; Elsevier: Amsterdam, The Netherlands, 2007; Volume 163, pp. 37–44.

26. Shen, J.; Ho, W.H.; Zhang, Y.; Liu, X.; Yao, Y.; Hildebrandt, D.; Abd El-Gawad, H.H.; Ali, H.M. Design of a Fischer-Tropsch Multi-Tube Reactor Fitted in a Container: A Novel Design Approach for Small Scale Applications. *J. Clean. Prod.* **2022**, *362*, 132477. [CrossRef]

27. Kibby, C.L.; Haas, A. Preparation of Cobalt-Ruthenium/Zeolite Fischer-Tropsch Catalysts. U.S. Patent 8,263,523, 11 September 2012.

28. Rensburg, H.V. Process for Preparing a Fischer-Tropsch Catalyst. U.S. Patent 9,387,463, 12 July 2016.

29. Zennaro, R.; Gusso, A.; Chaumette, P. Process for the Preparation of a Catalyst Based on Cobalt and Scandium. U.S. Patent 6,096,790, 1 August 2000.

30. Małecka, B.; Łącz, A.; Drożdż, E.; Małecki, A. Thermal Decomposition of D-Metal Nitrates Supported on Alumina. *J. Therm. Anal. Calorim.* **2015**, *119*, 1053–1061. [CrossRef]

31. Zhang, L.; Dong, L.; Yu, W.; Liu, L.; Deng, Y.; Liu, B.; Wan, H.; Gao, C.; Sun, K.; Dong, L. Effect of Cobalt Precursors on the Dispersion, Reduction, and CO Oxidation of CoO/γ-Al$_2$O$_3$ Catalysts Calcined in N2. *J. Colloid Interface Sci.* **2011**, *355*, 464–471. [CrossRef] [PubMed]

32. Mirzaei, A.; Arsalanfar, M.; Bozorgzadeh, H.; Samimi, A. A Review of Fischer-Tropsch Synthesis on the Cobalt Based Catalysts. *PCR* **2014**, *2*, 179–201. [CrossRef]

33. Arsalanfar, M.; Mirzaei, A.A.; Bozorgzadeh, H.R.; Atashi, H.; Shahriari, S.; Pourdolat, A. Structural Characteristics of Supported Cobalt–Cerium Oxide Catalysts Used in Fischer–Tropsch Synthesis. *J. Nat. Gas Sci. Eng.* **2012**, *9*, 119–129. [CrossRef]

34. Martinelli, M.; Gnanamani, M.K.; LeViness, S.; Jacobs, G.; Shafer, W.D. An Overview of Fischer-Tropsch Synthesis: XtL Processes, Catalysts and Reactors. *Appl. Catal. A Gen.* **2020**, *608*, 117740. [CrossRef]

35. Ernst, B.; Hilaire, L.; Kiennemann, A. Effects of Highly Dispersed Ceria Addition on Reducibility, Activity and Hydrocarbon Chain Growth of a Co/SiO$_2$ Fischer–Tropsch Catalyst. *Catal. Today* **1999**, *50*, 413–427. [CrossRef]

36. Steynberg, A.P.; Dry, M.E.; Davis, B.H.; Breman, B.B. Chapter 2—Fischer-Tropsch Reactors. In *Studies in Surface Science and Catalysis*; Steynberg, A., Dry, M., Eds.; Fischer-Tropsch Technology; Elsevier: Amsterdam, The Netherlands, 2004; Volume 152, pp. 64–195.

37. Weststrate, C.J.; Hauman, M.M.; Moodley, D.J.; Saib, A.M.; van Steen, E.; Niemantsverdriet, J.W. Cobalt Fischer–Tropsch Catalyst Regeneration: The Crucial Role of the Kirkendall Effect for Cobalt Redispersion. *Top. Catal.* **2011**, *54*, 811. [CrossRef]

38. Rytter, E.; Holmen, A. Deactivation and Regeneration of Commercial Type Fischer-Tropsch Co-Catalysts—A Mini-Review. *Catalysts* **2015**, *5*, 478–499. [CrossRef]

39. Khodakov, A.Y.; Chu, W.; Fongarland, P. Advances in the Development of Novel Cobalt Fischer−Tropsch Catalysts for Synthesis of Long-Chain Hydrocarbons and Clean Fuels. *Chem. Rev.* **2007**, *107*, 1692–1744. [CrossRef]

40. Mehrbod, M.; Martinelli, M.; Castro, J.D.; Alhraki, N.; Cronauer, D.C.; Kropf, A.J.; Marshall, C.L.; Jacobs, G. Fischer-Tropsch Synthesis: Direct Cobalt Nitrate Reduction of Promoted Co/Al$_2$O$_3$ Catalysts. *Catal. Today* **2021**, *369*, 129–143. [CrossRef]

41. Moodley, D.J.; Saib, A.M.; van de Loosdrecht, J.; Welker-Nieuwoudt, C.A.; Sigwebela, B.H.; Niemantsverdriet, J.W. The Impact of Cobalt Aluminate Formation on the Deactivation of Cobalt-Based Fischer–Tropsch Synthesis Catalysts. *Catal. Today* **2011**, *171*, 192–200. [CrossRef]

42. Visconti, C.G.; Lietti, L.; Tronconi, E.; Forzatti, P.; Zennaro, R.; Finocchio, E. Fischer–Tropsch Synthesis on a Co/Al$_2$O$_3$ Catalyst with CO$_2$ Containing Syngas. *Appl. Catal. A Gen.* **2009**, *355*, 61–68. [CrossRef]

43. Aldana, P.A.U.; Ocampo, F.; Kobl, K.; Louis, B.; Thibault-Starzyk, F.; Daturi, M.; Bazin, P.; Thomas, S.; Roger, A.C. Catalytic CO$_2$ Valorization into CH4 on Ni-Based Ceria-Zirconia. Reaction Mechanism by Operando IR Spectroscopy. *Catal. Today* **2013**, *215*, 201–207. [CrossRef]

44. Bobadilla, L.F.; Egaña, A.; Castillo, R.; Romero-Sarria, F.; Centeno, M.A.; Sanz, O.; Montes, M.; Odriozola, J.A. Understanding the Promotional Effect of Pt/CeO$_2$ in Cobalt-Catalyzed Fischer-Tropsch Synthesis Using *Operando* Infrared Spectroscopy at Moderated Pressures. *Fuel* **2022**, *312*, 122964. [CrossRef]

45. Liu, Y.; Jia, L.; Hou, B.; Sun, D.; Li, D. Cobalt Aluminate-Modified Alumina as a Carrier for Cobalt in Fischer–Tropsch Synthesis. *Appl. Catal. A Gen.* **2017**, *530*, 30–36. [CrossRef]

46. Bezemer, G.L.; Bitter, J.H.; Kuipers, H.P.C.E.; Oosterbeek, H.; Holewijn, J.E.; Xu, X.; Kapteijn, F.; van Dillen, A.J.; de Jong, K.P. Cobalt Particle Size Effects in the Fischer-Tropsch Reaction Studied with Carbon Nanofiber Supported Catalysts. *J. Am. Chem. Soc.* **2006**, *128*, 3956–3964. [CrossRef]